ISPRS Int. J. Geo-Inf. **2014**, *3*, 871-890; doi:10.3390/ijgi3030871

OPEN ACCESS

ISPRS International Journal of

Geo-Information

ISSN 2220-9964

www.mdpi.com/journal/ijgi/

Article

Rapid Prototyping — A Tool for Presenting 3-Dimensional Digital Models Produced by Terrestrial Laser Scanning

Juho-Pekka Virtanen [1,*], Hannu Hyyppä [1,2,4], Matti Kurkela [1], Matti Vaaja [1], Petteri Alho [1,3] and Juha Hyyppä [1,4]

1 School of Engineering, Aalto University, P.O. Box 15800, FI-00076 Aalto, Finland; E-Mails: hannu.hyyppa@aalto.fi (H.H.); matti.kurkela@aalto.fi (M.K.); matti.t.vaaja@aalto.fi (M.V.); petteri.alho@utu.fi (P.A.); juha.hyyppa@fgi.fi (J.H.)

2 Department of Construction and Real Estate, Helsinki Metropolia University of Applied Sciences, FI-00079 Metropolia, Finland

3 Department of Geography and Geology, University of Turku, FI-20014 Turun yliopisto, Finland

4 Finnish Geodetic Institute, P.O. Box 15, FI-02431 Masala, Finland

***** Author to whom correspondence should be addressed: E-Mail: juho-pekka.virtanen@aalto.fi; Tel.: +358-50-405-7791.

Received: 18 February 2014; in revised form: 20 June 2014 / Accepted: 23 June 2014 / Published: 4 July 2014

Abstract: Rapid prototyping has received considerable interest with the introduction of affordable rapid prototyping machines. These machines can be used to manufacture physical models from three-dimensional digital mesh models. In this paper, we compare the results obtained with a new, affordable, rapid prototyping machine, and a traditional professional machine. Two separate data sets are used for this, both of which were acquired using terrestrial laser scanning. Both of the machines were able to produce complex and highly detailed geometries in plastic material from models based on terrestrial laser scanning. The dimensional accuracies and detail levels of the machines were comparable, and the physical artifacts caused by the fused deposition modeling (FDM) technique used in the rapid prototyping machines could be found in both models. The accuracy of terrestrial laser scanning exceeded the requirements for manufacturing physical models of large statues and building segments at a 1:40 scale.

Keywords: rapid prototyping; TLS; 3D printing; FDM; 3D modeling; terrestrial laser scanning; point cloud, laser scanner

1. Introduction

Several applications in the fields of urban planning, construction, and cultural heritage require models that are at the same time accurate, visually pleasing, and easy to study, especially if the models are used for presentation and exhibition purposes.

Rapid prototyping (RP) techniques make it possible to easily manufacture physical models based on digital 3D models, meaning that model building is no longer a time-consuming, manual process. With RP, model making becomes an interesting and accessible tool for illustration [1,2]. RP techniques can be divided into additive and subtractive techniques, even though some authors only include additive techniques in RP [3]. With additive manufacturing techniques, such as stereolithography (SLA), the model is manufactured by adding material in layers [4]. Machining techniques, like milling, are subtractive techniques: The manufactured object is made by removing material from a block with a tool [5]. RP is widely used in industrial design, usually for making physical models [3]. In engineering, RP techniques have been used, e.g., in manufacturing tooling for sheet metal forming [6]. In addition, models made with RP have been used to validate simulation results [7] and visualize data obtained from Geographic Information Systems (GIS) [8]. To utilize RP, a triangle mesh model of the object is required [9]. This mesh model has to unambiguously define the internal volume of the object, so its surface has to be free of any holes. In design applications, this is created by tessellation from a CAD model. The resulting mesh model is sliced to determine the parallel horizontal cross sections of the model [9]. Based on these cross sections, the path that the machine is using in fabrication is calculated, typically this is referred to as a toolpath.

Additive manufacturing techniques used for RP include, for example, SLA, selective laser sintering (SLS), laminated object manufacturing (LOM), 3D printing and fused deposition modeling (FDM) [4,9,10]. In SLA, a directed laser beam is used to cure photo-curable resin, manufacturing the object in layers [4,9]. In LOM, the object is made by cutting and gluing layers of sheet material [4,9]. In 3D printing, a powder material is selectively bound with glue by an inkjet, forming the object in layers [4,9]. Fused deposition modeling (FDM) is one of the most common additive manufacturing techniques used in RP. With FDM, a heated thermoplastic material is extruded and used to build the model in layers (Figure 1) (e.g., see [4,9]). One of the advantages of FDM technology is that the machines can be used in a regular office environment, unlike for example SLA machines, where hazardous resins are used [10]. A disadvantage of FDM technology is that models require support structures during the manufacturing process, which have to be removed afterwards [10], in addition it cannot be used for manufacturing objects from metal materials. Typical build layer thicknesses for FDM range from 0.05 mm to 0.25 mm, producing a surface roughness of 56.6 μm Ra to 17.9 μm Ra, depending on the angle of the surface built [10]. The dimensional accuracy of a FDM print was found to be low compared to other RP methods, resulting in average linear dimensional accuracy of 95.3 percent [10].

In recent years, there has been a major change in the market of FDM machines. There are currently several, quite affordable, FDM machines available. Many of them are based on open-source projects. This has made RP equipment more accessible than ever before. The performance of one of these affordable RP machines has been studied by Pei *et al.* [11], who refer to these machines as Entry Level Rapid Prototyping (ELRP) machines. Typically, these machines use acrylonitrile butadiene styrene (ABS) or polylactic acid (PLA) as printing materials [12–16], ABS requiring a higher extrusion temperature [12]. Some of the models are capable of using two materials in the same print, to produce multi-colored models [12,13], while many only use one material at a time [14–16]. The build envelope of ELRP machines is dependent on the specific model, but typical values range from 100 mm by 100 mm by 125 mm [17] to 230 mm by 270 mm by 200 mm [12]. In addition to these ELRP machines being sold, there are also numerous service providers in the market offering RP as a service over the Internet (e.g., see [18,19]). When discussing RP by additive manufacturing, it has to be noted that occasionally the term "3D printing" is used to refer to all additive RP technologies. In a similar way, most RP machines are sometimes called "3D printers", even if they are based on a different technology, such as FDM.

Figure 1. The operating principle of Fused Deposition Modeling.

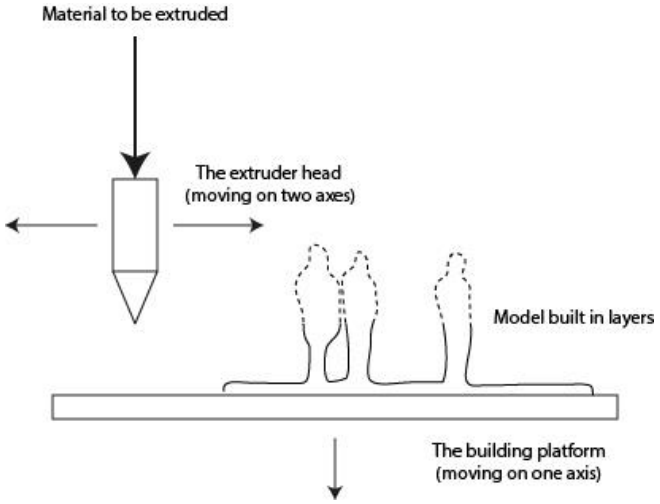

There are several different techniques for acquiring three-dimensional virtual models of the physical environment, for example photogrammetry and laser scanning (LS). Both of these are used extensively in the field of geo-information. Other methods also exist: A digital model can be created by measuring the key points of the original using, for example, a tachymeter if the geometry is simple enough. Existing drawings or plans can also be used in modeling, if they are available.

Photogrammetry is the technology of deriving 3D data, characteristics, and attributes from 2D images. Fraser [20], and Grün *et al.* [21], for example, have studied 3D modeling based on terrestrial images. Studies related to 3D modeling based on image sequences have been done, e.g., Bethmann *et al.* [22], and Cornelis *et al.* [23].

Static terrestrial laser scanning (TLS) can produce dense point clouds (up to hundreds of thousands of pts/m^2 from a range of 10 m). A specific TLS instrument has been demonstrated to reach an accuracy of 8 mm (in 92% of tests, 4 mm) or better in ranges of 10 m to 50 m [24]. By combining several scans, a larger point cloud can be created for the target [25]. TLS makes it possible to survey

built environments with great accuracy, great precision, and high spatial data intensity [26]. Studies by, for example, Arayici [26], Buckley *et al.* [27], Pu [28], and Pu and Vosselman [29], present approaches on how to use 3D modeling with TLS.

Mobile laser scanning (MLS) is an emerging technique, in which a laser scanning system is mounted on a vehicle. The vehicle might be, for example, a car or a boat and the measurements are made while the platform is moving. Global Navigation Satellite System (GNSS) and Inertia Measurement Units (IMU) are used for positioning and orienting the scanner. There have been several recent studies on MLS systems and their accuracy, as well as on environmental modeling done with MLS [30,31]. A relative accuracy of 10 mm or less has been reached with the Lynx Mobile Mapper system [32], making it possible to survey large areas with a very high detail level.

Point clouds obtained using laser scanning techniques are typically very large in size and contain up to hundreds of millions of points. Processing them requires computational resources and can also be rather time consuming [33]. Typical problems encountered when working with point clouds include gaps in the data caused by obstructions in the target and environment and varying point density in the data set (Figure 2).

Figure 2. The operating principle of Terrestrial Laser Scanning.

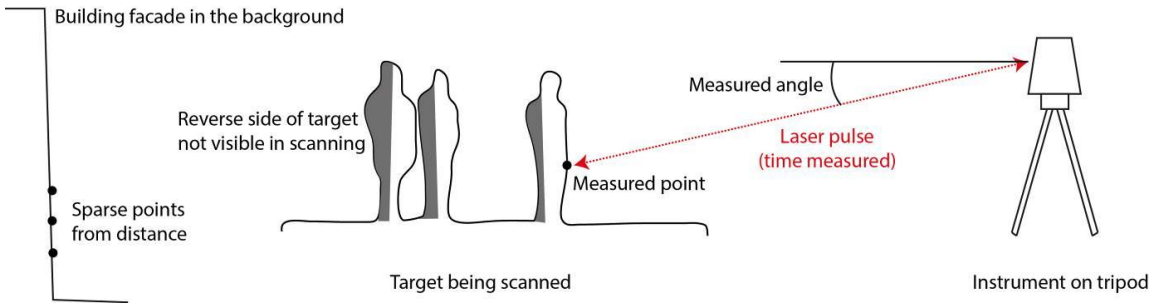

By combining 3D digitizing techniques with RP, physical models of the environment and artifacts can easily be made. The use of RP techniques also has the benefit that copies of the same model can easily be made [34]. These models have been used, for example, as demonstration and reconstruction models in archaeology [4,35,36], for making replicas of objects for museum purposes or preserving original artifacts [4,37], and as tactile models that make it possible for visually impaired users to study various targets [4,34,38]. These models can be made in either real size or to scale [4]. RP techniques can also be used to produce more sophisticated presentation models. With the use of color, more data can be included in the physical models. In a similar manner, three-dimensional legends can be added to help interpret the model [39]. The physical model can also be made from other data than just the three-dimensional geometry of a physical original; this approach has been presented by Rase [8,39] for visualizing data from geo-information systems.

Mesh models created by triangulating point clouds can also be used for RP. Some editing of the models is usually required to achieve a hole-free mesh model from 3D digitizing. The editing process can include stitching the scanned surfaces together, fixing of individual triangulation errors, filling holes in surface, and possibly splitting the model to be manufactured in pieces [4,5]. This editing can be performed with the Geomagic Studio software, for example [5]. This strategy was employed by Tucci *et al.* [5] to create sculpture replicas. In their case, the mesh model generation and editing

processes were performed using Geomagic Studio software. Models created with this method [5] reflect the original, 3D digitized targets quite closely, and they also include any possible surface errors, like dents, scratches, or other geometric defects from them if no additional mesh editing is performed.

ELRP machines have generated a certain amount of interest, and they increase the utilization of RP. In this study, we will test whether one of these ELRP machines based on FDM technology can be used to visualize the complex models produced by TLS. Based on the existing research, we can assume that this is possible with professional hardware [4,35,36], but not much research exists on the use of ELRP machines. Using the point clouds acquired with TLS, we will create the three-dimensional mesh models by triangulation. After this, we edit the mesh models to attain hole free models that can be used in RP. In addition, we aim to gain practical experience with using an ELRP machine. To compare the workflow and the quality of the results, we present two cases. In the first case, we utilize an older, professional-quality RP machine and in the second case we use a new ELRP machine. In both cases, TLS is used to acquire the models to be manufactured.

2. Cases

2.1. Segment of Façade from Grönqvist's Building

The façade of the Grönqvist's building, which is in the Neo-Renaissance style (Figure 3), is said to be one of the most complex façade in the city of Helsinki, Finland. We used a Leica HDS6100 terrestrial laser scanner to measure the façade. The HDS6100 is a 690 nm, phase-based, continuous-wave laser scanner with a $360° \times 310°$ field of view. The distance measurement accuracy for it is ±2 mm at a distance of 25 m. The circular beam diameter at the exit and the beam divergence are 3 mm and 0.22 mrad, respectively. In the "High" resolution setting, the HDS6100 produces a point spacing of 6 mm on an orthogonal target at 10 m distance from the scanner. With the "Super high" setting, the corresponding spacing is 3 mm. In total, the façade was measured from four separate TLS scanning positions. Three of the measurements were done using the "High" resolution setting, and one with the "Super high" setting, producing a higher point density. All measurements were taken with the instrument mounted on a tripod, from the street level. TLS measurements were collected in the multiscan mode and the objective of the measurements was to obtain the best possible point coverage for the target. The reference targets were placed around the study area for point cloud registration. The TLS point clouds were co-registered using sphere reference targets, with the Leica Cyclone software. The resulting average overlap errors for the four scans were: 0.012 m, 0.007 m, and 0.011 m. In total, 364 million points were measured from the area. The façade was separated from the data set; it contained 46 million points.

For creating a mesh model from the point cloud Geomagic Studio 11 was used. The selected area of the façade was segmented using the combined point clouds of the façade (shown in Figure 3). The excess points were removed by manual selection, including the surface of the sidewalk along the lower edge of the façade, which was also visible during the scanning. In total, 2,119,631 points were used for the triangulation. The triangulation was performed with the "Wrap" function, during which noise reduction was performed with the "Medium" setting. The density of the polygon mesh was reduced with the "Decimate" function. After this, the gaps remaining in the mesh were filled using the

"Fill holes" tool (Figure 4). The filling was performed manually, hole by hole, using the "Curvature" type fill. This was the most laborious part of the process. Finally, the model was edited to a solid mesh model by extruding the mesh edges and adding a straight back surface to the model (Figure 3.). A similar procedure was carried out for the visible windows in the doors in the data set.

Figure 3. (**a**) The façade of the building; (**b**) the obtained point cloud; (**c**) the completed mesh model.

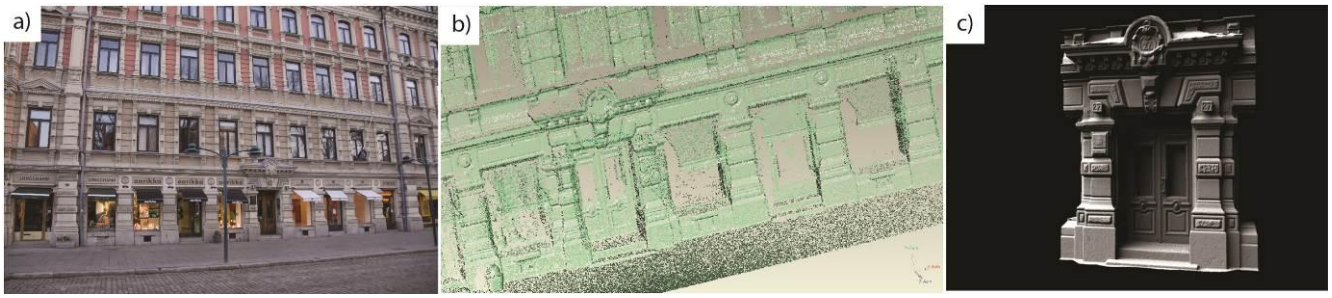

Figure 4. A segment of the mesh before and after decimation and filling holes.

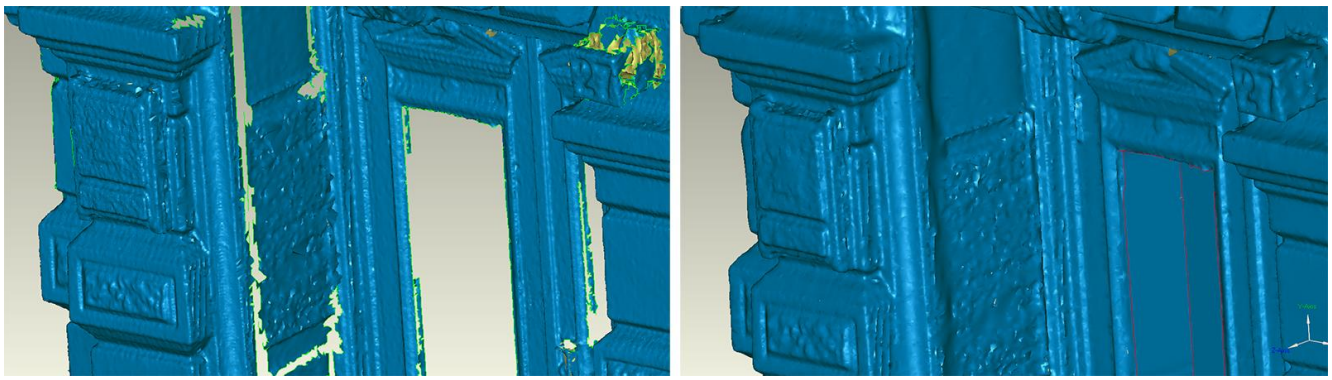

2.2. Statue at the University of Turku Campus

The "Three Witty Men" statue was made by the sculptor Harry Kivijärvi in 1968. It is located at the University of Turku. The statue was digitized (Figure 5a) as a part of a larger survey project, which covered most of the main buildings on campus. We scanned the statue using the same instrument as in the first case. A larger number of terrestrial laser scans were taken from the area, two of which were used to model the statue (Figure 5b). They were taken with the same "High" resolution setting as in the first case. In total, they consisted of 57 million points. Three spherical reference targets were placed around the statue for point cloud registration. The point clouds were co-registered with the Z + F software, with the resulting average error being 0.012 m. The Figure 5b provides an overview of the measured area from a top projection in the vicinity of the statue.

Figure 5. (**a**) Laser scanning the statue; (**b**) top view of the area showing the scanning positions.

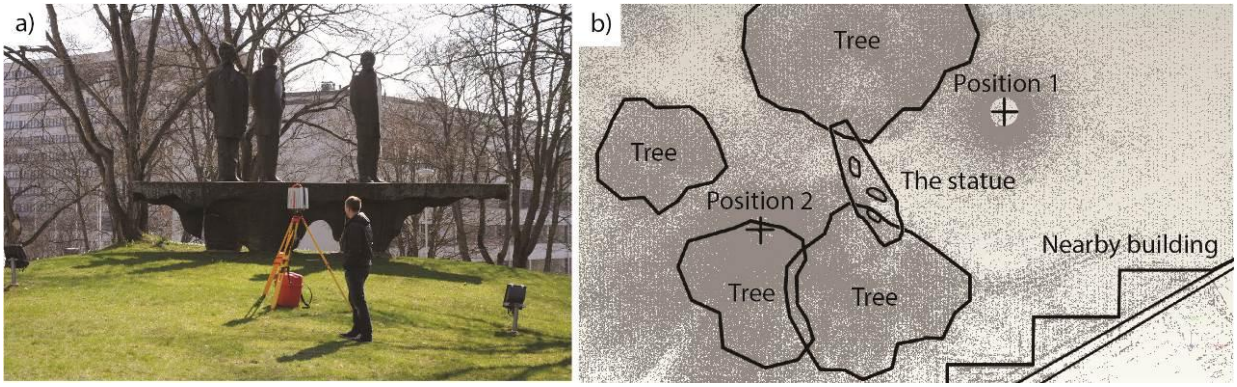

The 3D mesh model of the statue was built from two TLS point clouds, using again Geomagic Studio 11 software. A total of 1.3 million points were used for the modeling. Points not belonging to the target were removed manually and the point clouds were filtered to remove the outlying points, using the "Select outliers" tool. After further segmentation, 1,040,824 points were used for triangulation. Noise reduction was applied during the triangulation process, as in the first case. The resulting triangle meshes were combined, and surface editing tools were used to fill holes remaining in the mesh (Figure 6). During this process, the upper surface of the pedestal of the statue had to be modeled based on the edges of the pedestal as it was not visible in the terrestrial laser scans. This was done with the "Fill holes" tool, using the "Flat" fill type and selecting the edges of the mesh in segments. The gaps in the sides of the figures also had to be filled this way, using the "Curvature" fill type of the "Fill holes" tool. This editing process was, again, the most laborious part of the process.

Figure 6. (**a**) The triangulated point clouds colored according to normal direction, with outside facing normals marked in blue; (**b**) Constructing a surface to the top of the pedestal. Segments of mesh edges have been selected, and the new surface to be created is marked in red; (**c**) The mesh after editing.

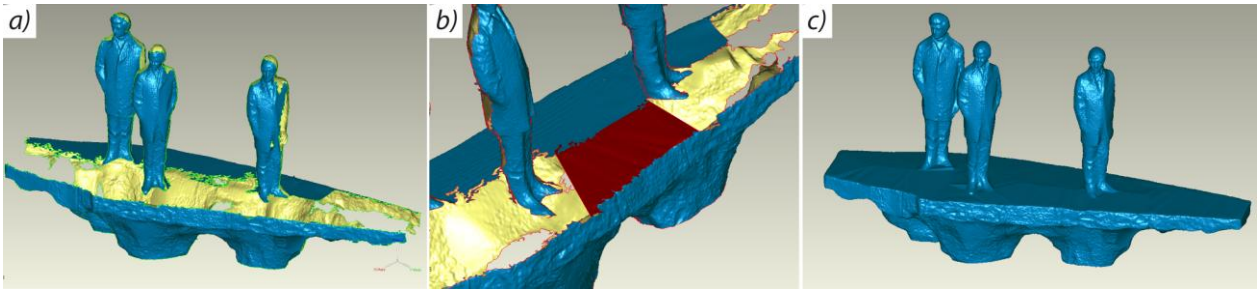

3. Evaluation Methods

Since we will discuss both our experiences with two different RP machines, and the quality of the results achieved with them, we have chosen to evaluate the original data sets, the manufacturing process, and the completed models (Figure 7).

Figure 7. Workflow (**a**); and evaluation steps (**b**).

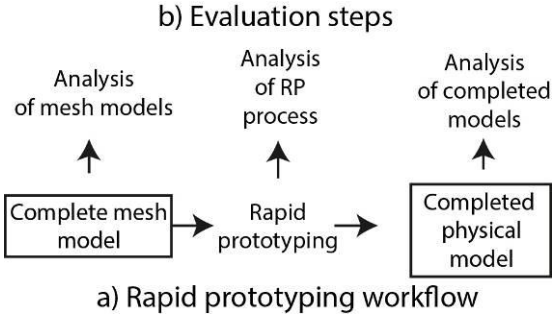

3.1. Evaluating the Mesh Models

We chose to perform a set of comparisons since we had used two different data sets. We did this to identify potential differences in the mesh models that could affect our comparison of the two machines. For the algorithmic evaluation of the complexity of the 3D mesh models, we used methods introduced by Valentan *et al.* [40]. These methods are extremely simple, and, therefore, they may not always produce accurate results [40]. We began by making an extremely simple estimation, where complexity (C_1) is described by the amount of triangle facets (n) in the model:

$$C_1 = n \tag{1}$$

For the second method, we calculated the ratio between the model volume (v) and number of triangle facets in the mesh (n):

$$C_2 = \frac{v}{n} \tag{2}$$

Third, we calculated the ratio between the volume of the model and the surface area (a) of the model:

$$C_3 = \frac{v}{a} \tag{3}$$

3.2. Evaluating the Rapid Prototyping Process

To evaluate the two different RP machines, we mapped the process steps in both cases. By identifying any possible extra steps in the manufacturing process caused by differences in the equipment, we were able to compare the usability and utility of these machines in practice. In an optimal situation, the RP should be a one-step process, where the model is made without any preliminary steps and no modification of the model is required after manufacturing. In practice, there are typically some finishing steps after RP with FDM technology, for example removing support material from the model [4].

3.3. Evaluation the Completed Models

To evaluate the visual quality of the physical models, we identified possible surface errors and other three-dimensional artifacts caused by the RP machines. These artifacts may have included visible steps, extra shapes, or gaps in the model. To document the artifacts, we used digital macro photography with a Nikon D800E DSLR camera, which had a sensor resolution of 7360 × 4912 pixels, a physical

sensor size of 35.9 × 24 mm, and a macro-lens with a focal length of 105 mm and an aperture value of F 4.92 when producing a maximum reproduction ratio of 1:1. We photographed the physical models in artificial lighting, using an exposure time of 1/100 s and an aperture of F 10.0. In an optimal case, the model should be as close to the original mesh model as possible, and, therefore, it should not be possible to observe the artifacts.

To evaluate the accuracy of the models when compared to the original mesh models used for calculating the toolpaths, we 3D-digitized the models and compared the original mesh model to the scanned surface of the model made with the RP machine. We used a Konica Minolta Vivid 9i 3D laser scanner to 3D digitize the physical models. The scanner is based on laser triangulation. It projects a moving stripe of monochromatic light on the object being scanned, via a galvano mirror. The deformation of the projected stripe is captured by the devices' internal camera, having an 8.46 mm CCD sensor with 340,000 pixels. The cameras image can also be used to capture the texture of the object being scanned. Lenses of different focal lengths can be used with the devices' camera to change the size of the measured area. The accuracy of digitizing is ± 0.05 mm when using a f = 25 mm lens at a distance of 0.6 m, the measuring area being 111 mm by 83 mm. Before scanning, the device is calibrated using the field calibration system. To facilitate scanning, a rotating stage platform can be used to automatically rotate the object being scanned.

4. Results

4.1. Segment of Façade from Grönqvist's Building

We manufactured the model of the façade segment out of white ABS plastic using an older, professional-quality RP machine (Table 1). We calculated the toolpaths using the manufacturer's software suite. We built the model using support structures, which were removed via an ultra-sonic cleaner afterwards. After this, the model was painted since the white color of the material made it difficult to study the surface geometry in detail.

Table 1. Specifications of the rapid prototyping machines used.

Case	**Grönqvist's Building**	**Grönqvist's Building**	**Statue**
Manufacturer	Stratasys	Ultimaker	Ultimaker
Model	Prodigy Plus	Ultimaker Kit (BETA)	Ultimaker Kit (BETA)
Build envelope size	203 × 203 × 305 mm	210 × 210 × 220 mm	210 × 210 × 220 mm
Build material used	ABS plastic	PLA plastic (white)	PLA plastic (metallic gray)
Software used to generate toolpaths	Stratasys Insight	Netfabb Studio Basic for Ultimaker 4.9	Cura 12.08
Layer thickness used in manufacturing	0.245 mm	0.150 mm	0.200 mm
Software used in mesh modeling	Geomagic Studio 11, 64 Bit Edition	Geomagic Studio 11, 64 Bit Edition	Geomagic Studio 11, 64 Bit Edition
Total amount of facets in mesh model	1,322,068	1,322,068	2,224,986

The same mesh model was also used to manufacture the model with an Ultimaker ELRP machine from white PLA material. Netfabb Studio for Ultimaker 4.9 was used to calculate the toolpaths. The model was built with the backside down, resulting in a relief-like geometry that did not require support structures. After the manufacturing, extra threads of the plastic material, and a platform shape left by the machine were removed manually (Figure 8). No further finishing of the model was performed.

4.2. Statue at the University of Turku Campus

We made the model out of PLA plastic material using an ELRP machine (Table 1). We created toolpaths using open-source software. Since the ELRP machine being used only supported manufacturing with one material at the time, meaning that it was not possible to make dissolvable support structures, we decided to split the 3D model into two components before manufacturing. By splitting the model along the pedestal of the statue, both of the pieces were relatively relief like and possible to manufacture without support structures. Figure 9a shows the segmentation of the model. We made the upper part and the lower part of the model separately, with the lower part (in blue color) being manufactured upside down (Figure 9). After RP, both parts of the model were finished manually with a knife, removing all material not belonging to the model, such as extra threads of plastic left by the ELRP machine. Once completed, the pieces were joined with glue. No further finishing was applied to the model's surface.

Figure 8. The model before (**a**) and after (**b**) manual cleaning, with detail images (**c**,**d**).

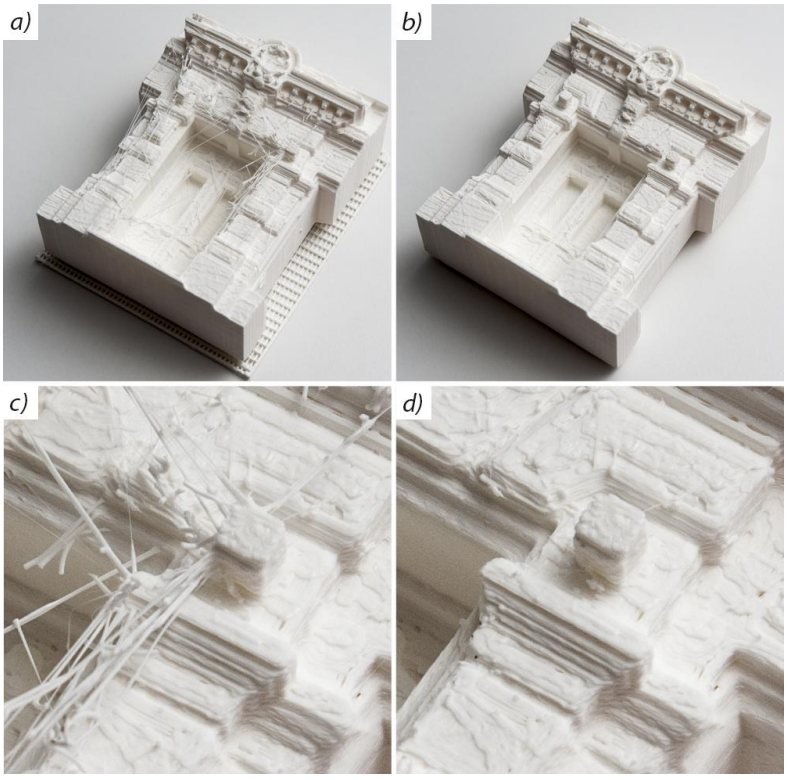

Figure 9. (**a**) Both parts of the completed mesh model, with the lower part shown in blue, (**b**) the top part of the model in the ELRP machine; (**c**) and the completed physical model.

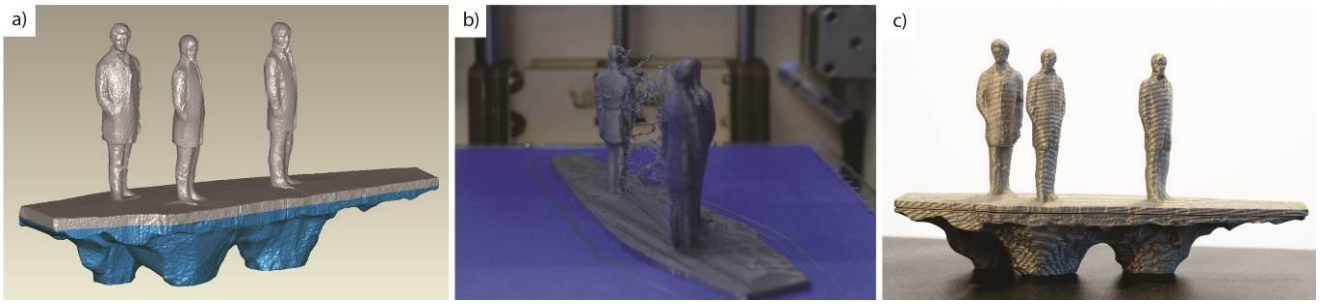

4.3. Analyzing the Data Sets Used

Since both models were made to scale, we calculated the ratios mentioned in the scales at which they were made. The results (Table 2) are difficult to interpret, but not conflicting. Both the C_1 and C_2 are lower in the statue data set, indicating a higher level of complexity for both calculation methods. This reflects the shape of the models, where the façade segment is more a single body volume and the statue model consists of more separate, but connected, volumes.

The number of triangles in the mesh is independent of the scale of the model. Valentan *et al.* [40] considered a model with roughly 500,000 facets complex, where simple meshes only contained several hundred triangles. Compared to this, both of our models were extremely complex, even though they were considerably different in terms of the number of triangles. This reflects the complexity of the mesh models obtained with TLS.

Table 2. Dimensions, scales and calculated complexity indexes of the created models.

Parameter	Statue Mesh Model	Façade Segment Mesh Model
Bounding box (mm)	54 × 188 × 107	99 × 119 × 55
Scale (to real measured target)	1:40	1:40
Amount of triangles in mesh	2,224,986	1,322,068
Mesh surface area (mm^2)	30,157.2	47,762.6
Mesh volume (mm^3)	145,749.0	355,536.2
$C_2 = v/n$	0.066	0.437
$C_3 = v/a$	4.833	7.444

4.4. Analyzing the RP Process

As we studied the processes for making the physical models (Figure 10), it became apparent that the process was most complex in the case of the statue model. The steps used for data acquisition and mesh modeling were similar. In all cases, the models were edited to fill holes in the mesh. After the mesh model had been completed, the processes were different. Since we had decided to manufacture the statue model in two segments, we needed to include an extra modeling step, in which the model was segmented and solid mesh models were created from each segment. After this, we made the model in two pieces, which were finished manually and then joined. This would not have been necessary with the professional machine that supported the creation of support material removable by ultra-sonic

cleaner. The differences in geometry therefore placed some restrictions on the way in which the model was manufactured when using the ELRP machine. As the geometry of the façade segment model was different, and permitted the manufacturing without support structures, it was possible to manufacture the model with the ELRP machine without segmentation. With the façade segment model manufactured with the professional machine, we decided to paint the model to achieve a better definition of shape via light and shadow in the final model.

4.5. Analyzing the Completed Models

When looking at the machine-induced artifacts, the models are quite similar. Layers, a step pattern, and over extrusion, and holes can be seen in all models (Table 3). These perhaps characterize the FDM as a technique. The lack of supporting material and the less controllable extrusion of the ELRP machine are visible as gaps in the layers, and some hanging layers are visible in the statue model (Figure 11). The gluing seam is clearly visible in the statue model because of slight warping of the models. In terms of accuracy and surface quality, the differences were not significant. A modern ELRP machine based on FDM could, in our experiments, reach the same degree of visually evaluated surface quality as an older, professional-quality machine. The smaller layer height used in the ELRP machine in these tests rendered the ELRP machines' layers less visible.

Figure 10. Comparison of rapid prototyping processes at different stages: (**a**) TLS stage; (**b**) Modeling stage; (**c**) Rapid prototyping stage; and (**d**) Finishing stage.

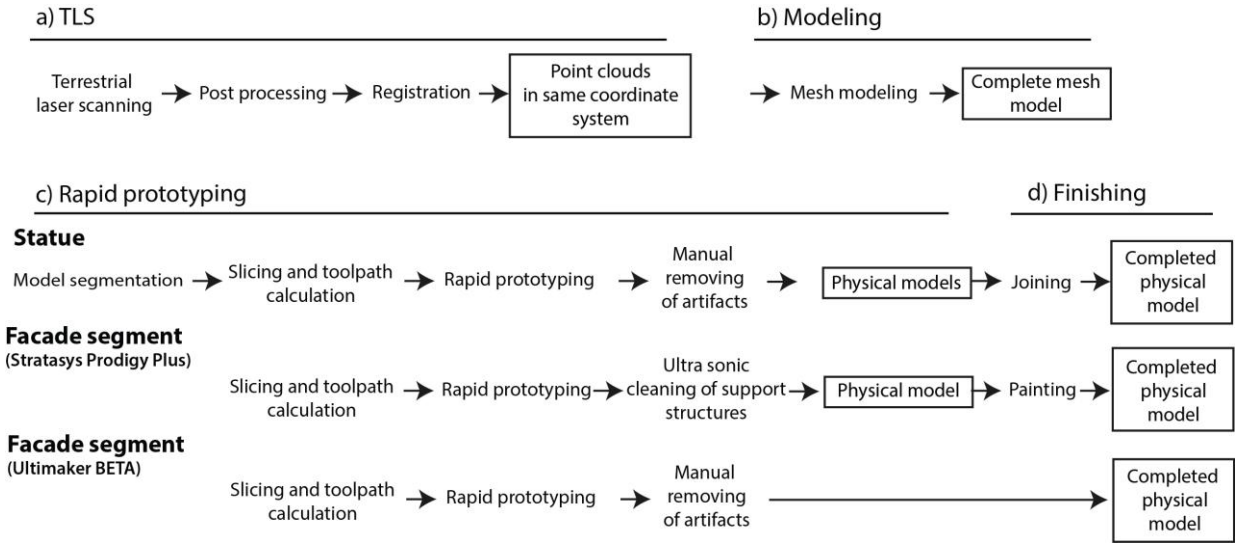

Table 3. Visible artifacts caused by rapid prototyping (RP) machines found in the models.

Type of Artifact	Façade Segment Model (Stratasys Prodigy Plus)	Façade Segment Model (Ultimaker BETA)	Statue Model
Visible layers	X	X	X
Step pattern	X	X	X
Hanging layers			X
Gaps in layers		X	X
Over/under extrusion	X	X	X
Seam			X

Figure 11. Different artifacts caused by RP machines: (**a**) Seam; (**b**) Hanging layers; (**c**) Visible layers; (**d**) Gaps in layers; (**e**) Over/under extrusion; (**f**) Step pattern.

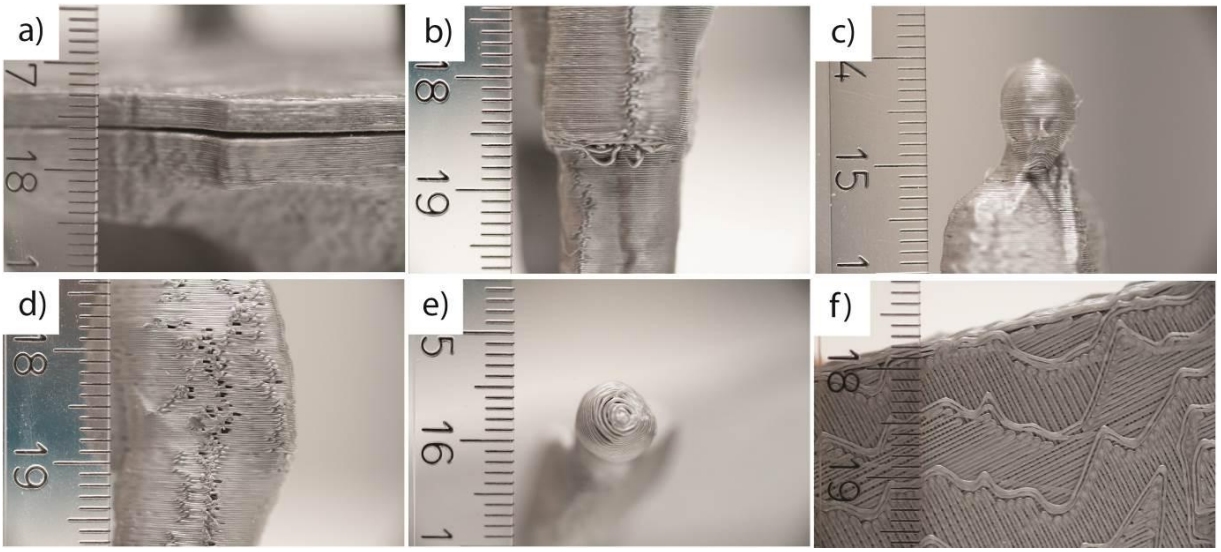

To verify the dimensional accuracy of the manufactured models, we 3D digitized all models using the specified Konica-Minolta Vivid i9, non-contact digitizer. In all cases, we digitized the models in 12 segments, with the object rotated 30 degrees between scan positions around the Z-axis (height). All models were digitized using the f = 14 mm lens. The scanning was performed using the Konica Minolta Polygon Editing Tools software, which triangulates the scans directly after scanning. The individual scanned mesh surfaces were then exported in stl format. The scans were registered in Geomagic Qualify 11 software using the "Global Registration" tool. The average distances between scans were 0.11 mm with the standard deviation of 0.17 mm in the façade model case manufactured with the Stratasys Prodigy machine, 0.08 mm and 0.14 mm for the same model manufactured with the Ultimaker, and 0.12 mm and 0.25 mm for the statue model. The scans were combined with the "Merge" tool, after which the resulting mesh models were used in the deviation analysis.

The models were co-registered with the original mesh model that was used in toolpath calculation using the "Global Registration" tool. In the façade segment model manufactured with the Prodigy Plus machine, the average distance was 0.43 mm and standard deviation 0.31 mm. In the façade segment model manufactured with the Ultimaker the corresponding values were 0.25 mm and 0.26 mm. In the Statue model case, the average distance was 0.33 mm and the standard deviation 0.28 mm. The calculated 3D deviations are in Table 4.

Table 4. 3D Deviations.

Model	Statue	Façade Segment (Prodigy Plus)	Façade Segment (Ultimaker BETA)
Standard deviation	0.35 mm	0.42 mm	0.36 mm
Average deviation (+/−)	+0.19/−0.36 mm	+0.51/−0.28 mm	+0.25/−0.23 mm

Figure 12. Deviation analysis and scatter of the Fa çade segment model (Stratasys Prodigy Plus).

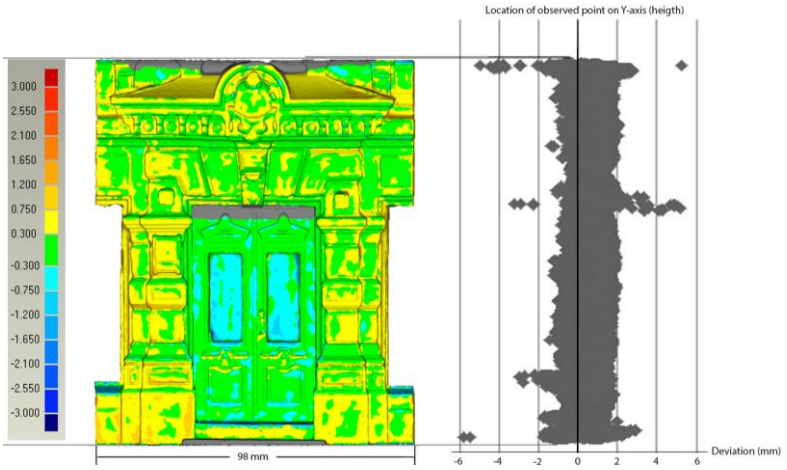

Looking at the results of deviation analysis (Table 4), the standard deviation was largest in the Fa çade segment model manufactured with the older, professional FDM machine. The visualized results (Figure 12), and the high positive average deviation confirm this. The model is too large. This is most likely caused by the manufacturer's toolpath calculation software scaling the model slightly to make it possible to sand the FDM layer steps away without causing a considerable error in the final measurement. We did not perform this sanding, and it is visible in the results. The scattering of deviations is less even, and observed deviations are larger in the fa çade segment model manufactured with the ELRP machine (Figure 13). This indicates more variation in model details, caused by FDM surface errors, such as over- and under extrusion. Looking at the positive and negative average deviations, and the scattering of deviations, the scale of the model is more correct in this model, than in the one manufactured with the older professional machine.

Figure 13. Deviation analysis and scatter of the Fa çade segment model (Ultimaker).

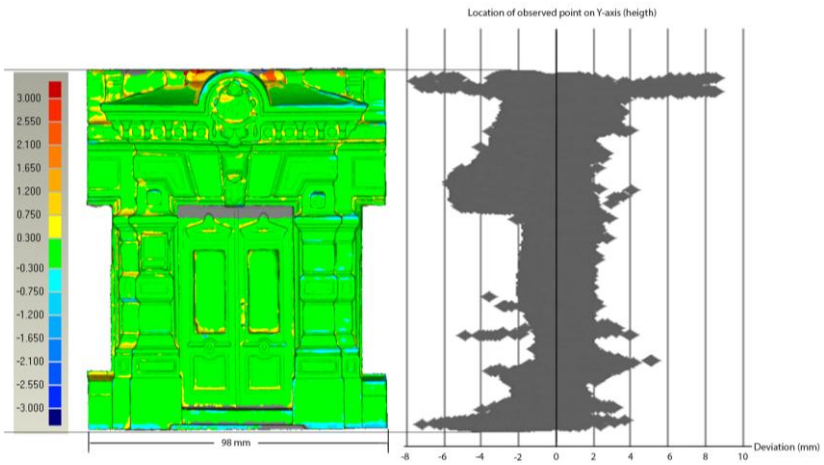

The deviation scatter of the statue reveals, first, a slight misalignment of the two glued components. In Figure 14, we can see how the top part of the pedestal is just a bit too much on the left. The seam is also visible. The higher deviations in the left-most figure in the statue were caused by the model being damaged during storage and transport. The figure is not completely attached to the pedestal. This can also be observed in the deviation scatter, the deviations of the figure increasing with height.

The average deviations may indicate the model being slightly too small, this can also be observed in the deviation scatter.

Figure 14. Deviation analysis and scatter of the Statue model.

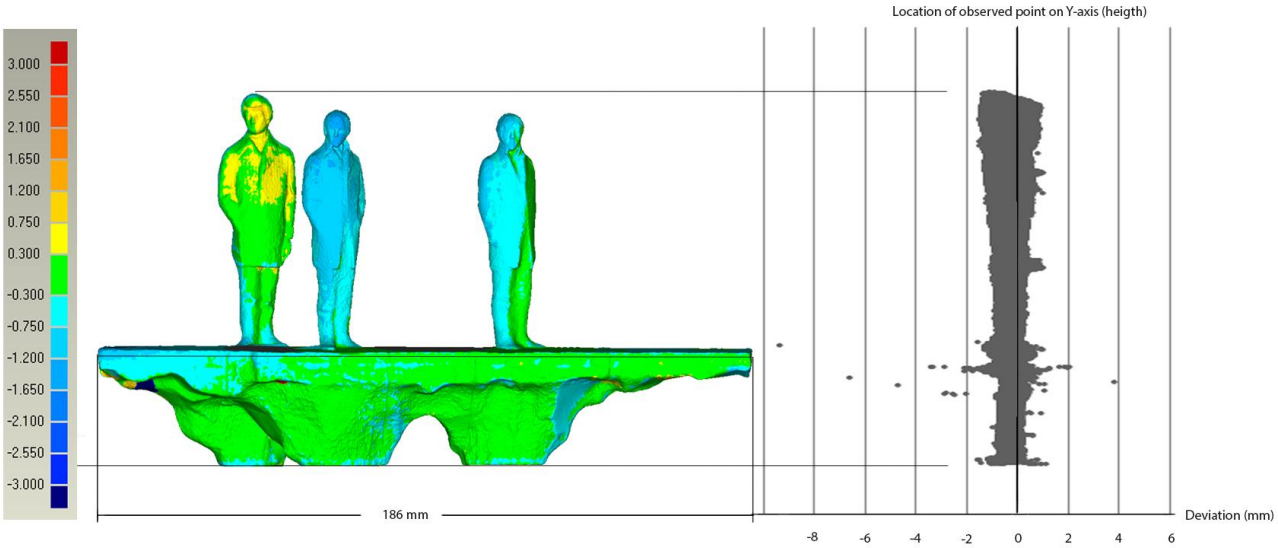

5. Discussion and Conclusions

Recent developments in terms of the affordability of FDM machines have changed the field of RP. With the emergence of ELRP machines, RP has become more available to users than ever before. In this paper, we looked at how RP technology is currently being used, namely FDM, to manufacture physical models from three-dimensional data sets obtained with TLS.

We tested RP with two different laser-scanned data sets and two different RP machines, both based on FDM technology. A traditional, professional-quality RP machine was used in the first case. In the second case, the model was manufactured with an ELRP machine.

The data sets were different in terms of their algorithmic and perceived complexity. The complexity of the statue data set was significantly greater with all of the estimation methods used: It had a 68% higher triangle count and its complexity indexes were only 15% and 64% of the complexity indexes for the fa çade segment data set, indicating a higher degree of complexity.

It was possible to manufacture the models in both cases, but in the statue model case the model had to be made in two parts. This was because the ELRP machine was unable to create removable support structures for the object during the manufacturing process, and unsupported shapes could therefore not be made. The process of splitting the model of the statue before manufacturing illustrated the trade-offs that become necessary when utilizing ELRP machines. The other alternative method would have involved making manually removable support structures from the same material as the model. In this case, the professional-quality RP machine offered a higher degree of geometric freedom during manufacturing. Evaluating the manufacturability of solid mesh models is clearly dependent on the chosen RP technology and its characteristics as well as the model's geometry. The complexity of the model does not necessarily affect the ability to manufacture it with an RP machine. More attention had to be paid to the orientation and geometric properties of the model when manufacturing it with the ELRP machine. This highlights the need for obtaining more experience in using ELRP machines.

Because it was possible to remove the support material with an ultra-sonic cleaner used in the professional-quality machine, there was less manual work in finishing the model manufactured with it. All models have visible artifacts caused by the RP manufacturing technology. More of these artifacts can be found in the models made with the ELRP machine. However, the results that we obtained with a single ELRP machine cannot be generalized to all ELRP machines, since there are several different models available. Some of them, for example, have a dual extrusion system, enabling the extrusion of removable support structures.

Looking at the accuracy of models, the data acquisition can be performed by TLS with the accuracy of a few mm. With the Leica HDS6100 the ranging accuracy is reported by manufacture to be ±2 mm. In addition to the instruments accuracy, the co-registering of point clouds affects the accuracy of the data set obtained. In our cases, the largest co-registration average overlap error of two scans was found to be 12.46 mm. In a model made to scale of 1:40, this creates an error of roughly 14 mm/40 = 0.35 mm in the final model. The deviations caused to the models by the manufacturing were similar or larger, ranging from 0.35 mm to 0.42 mm. The accuracy of the 3D digitizing instrument used in measuring models was ±0.05 mm, as reported by the manufacturer. In the 1:40 scale used, the errors caused by the TLS are comparable or smaller than the observed errors of FDM manufacturing, making TLS a well-suited method for acquiring virtual models that can be used to manufacture physical representations. The FDM machines could be used to create illustrative models, with a few centimeters accuracy in targets' real world size.

Since a single material RP machine was used in both cases, the physical models produced were mono-colored. Colored physical models could have been made by using a different RP technique [34], such as powder-based devices (e.g., [41]). However, it would have been necessary to acquire texture images from the digitized targets to obtain color information. In our case, only the laser intensities were recorded.

One alternative to buying and operating ELRP machines is to subcontract. There are service providers offering RP over the Internet that use different additive manufacturing technologies [18,19]. The choice between using subcontractors *versus* owning and operating the machines is a difficult one. When using a service provider, all of the setup work and machine maintenance work are also subcontracted. Neither, does the client have to spend time manufacturing the model. On the other hand, the delivery times need to be taken into the account and price of the models is higher. In "one-off" models, using service providers is an interesting option. If RP becomes more commonly used as an illustration tool in the projects, the decision will be more difficult. In both of our cases, the file size of the models was too large to be easily ordered from these services.

Successfully using RP technologies to visualize complex, three-dimensional models have been studied by many authors. The technologies have been used to visualize geometrically complicated objects [4,34]. In some cases, the original targets have been documented using TLS [4]. Clearly, RP machines can be used to visualize three-dimensional models produced with TLS. However, the process of using RP machines is often not documented, making it impossible to estimate how easy it actually is to use the techniques [4,34]. In addition, there is very little research on using ELRP machines in this manner; in most reported cases, professional-quality machines have been used. It was fascinating to see that a modern, affordable RP machine could achieve the same surface quality and level of detail as a traditional professional machine. New 3D-digitizing methods, such as

backpack-based MLS [42], make it possible to efficiently survey large and geometrically complicated outdoor and indoor environments. New presentation methods are needed to communicate the measured results in a simple manner. ELRP machines offer an interesting possibility for doing so in this particular field. With the price of machinery such as this being quite low already, we expect to see an increase in the use of RP-made models in a variety of purposes, including the visualization of 3D models obtained via 3D-digitizing methods.

Acknowledgments

This research project was supported by the Academy of Finland (CoE-LaSR), the Centre of Excellence in Laser Scanning Research (project number 272195), the Academy of Finland RivCHANGE project (project number 272711), The Finnish Funding Agency for Innovation (Tekes) ÄRY project, the Aalto Energy Efficiency Research Programme (Light Energy—Efficient and Safe Traffic Environments project), Research on Resident-Driven Infill Development Possibilities—Case Study in Urban Areas in Finland (REPSU), Aalto University doctoral program and the EUE project (project number 2141226). The authors wish to thank the Aalto University School of Arts, Design and Architecture's Department of Design for the 3D print of the Grönqvist building.

Author Contributions

Juho-Pekka Virtanen was the main author of the article and made the analyses. Hannu Hyyppä, Matti Kurkela and Matti Vaaja were responsible for the TLS measuring campaigns. The article was improved by the contributions of all the co-authors at various stages of the analysis and writing process.

Conflicts of Interest

The authors declare no conflict of interest.

References

1. Sass, L. Rapid Prototyping Techniques for Building Program Study. In Proceedings of the 9th International Conference on Computer Aided Architectural Design Research in Asia (CAADRIA '04), Seoul, Korea, 28–30 April 2004; Lee, H.S., Choi, J., Eds.; Institute of Millennium Environmental Design and Research, Yonsei University and the Korean Housing Association: Seoul, Korea, 2004; pp. 655–670.
2. Celani, G.; Piccoli, V. The roles of a model. *Arquiteturarevista* **2010**, *6*, 50–62.
3. Chua, C.K.; Chou, S.M.; Wong, T.S. A study of the state-of-the-art rapid prototyping technologies. *Int. J. Adv. Manuf. Technol.* **1998**, *14*, 146–152.
4. Tucci, G.; Bonora, V. From Real to ... "Real". A Review of Geomatic and Rapid Prototyping Techniques for Solid Modelling in Cultural Heritage Field. In Proceedings of the ISPRS Trento 2011 Workshop, Trento, Italy, 2–4 March 2011; Remondino, F., El-Hakim, S., Eds.; Copernicus GmbH: Göttingen, Germany, 2010; Volume XXXVIII-5/W16.

5. Tucci, G.; Bonora, V. Application of High Resolution Scanning Systems for Virtual Moulds and Replicas of Sculptural Works. In Proceedings of the Twenty-First CIPA Symposium, Athens, Greece, 1–6 October 2007; Copernicus GmbH: Göttingen, Germany, 2007; Volume XXXVI-5/C53, pp. 721–726.
6. Mueller, D.H.; Mueller, H. Experiences Using Rapid Prototyping Techniques to Manufacture Sheet Metal Forming Tools. In Proceedings of the ISATA Conference, Dublin, Ireland, 25–27 September 2000.
7. Yang, T.; Buswell, R.A.; Cook, M.J. Exploring Rapid Prototyping Techniques for Validating Numerical Models of Naturally Ventilated Buildings. In Proceedings of the 12th International IBPSA Conference, International Building Performance Simulation Association, Sydney, Australia, 14–16 November 2011; pp. 965–971.
8. Rase, W.-D. Physical Models of GIS Objects by Rapid Prototyping. In Proceedings of the ISPRS Commission IV, Symposium 2002, Ottawa, ON, Canada, 9–12 July 2002; Armenakis, C., Lee, Y.C., Eds.; Volume XXXIV, Part 4.
9. Yan, X.; Gu, P. A review of rapid prototyping technologies and systems. *Comput. Aided Des.* **1996**, *28*, 307–318.
10. Upcraft, S.; Fletcher, R. The rapid prototyping technologies. *Assem. Autom.* **2003**, *23*, 318–330.
11. Pei, E.; Campbell, R.I.; de Beer, D. Entry-level RP machines: How well can they cope with geometric complexity? *Assem. Autom.* **2011**, *31*, 153–160.
12. Creatr. Available online: https://www.lpfrg.com/product/creatr/ (accessed on 12 May 2014).
13. Cube 3D Printer. Available online: http://cubify.com/en/Cube/TechSpecs (accessed on 12 May 2014).
14. Ultimaker 2 Our Latest 3D Printer. Available online: https://www.ultimaker.com/pages/our-printers/ultimaker-2 (accessed on 12 May 2014).
15. Solidoodle 3D Printer, 3rd Generation. Available online: http://store.solidoodle.com/index.php?route=product/product&product_id=79 (accessed on 12 May 2014).
16. R1 "ABS + PLA Model" 3D Printer. Available online: http://www.robo3dprinter.com/collections/3d-printers/products/robo-3d-abs-model-fully-assembled (accessed on 12 May 2014).
17. Makerbot Replicator Mini. Available online: http://store.makerbot.com/replicator-mini (accessed on 12 May 2014).
18. 3D Printing Service i.materialise. Available online: http://i.materialise.com/ (accessed on 3 December 2013).
19. Shapeways—Make, Buy, and Sell Products with 3D Printing. Available online: http://www.shapeways.com/ (accessed on 3 December 2013).
20. Fraser, C.S. Network Design. In *Close-Range Photogrammetry and Machine Vision*; Atkinson, K. B., Ed.; Whittles Publishing: Caithness, UK, 1996; pp. 256–282.
21. Grün, A.; Remondino, F.; Zhang, L. 3D Modeling and Visualization of Large Cultural Heritage Sites at Very High Resolution: The Bamiyan Valley and Its Standing Buddhas. In Proceedings of the XXth ISPRS Congress Technical Commission V, Istanbul, Turkey, 12–23 July 2004; Altan, O., Ed.; Volume XXXV Part B5, pp. 603–608.

22. Bethmann, F.; Herd, B.; Luhmann, T.; Ohm, J. Free-Form Surface Measurement with Image Sequences Under Consideration of Disturbing Objects. In *Optical 3D Measurement Techniques*; Technical University Vienna: Vienna, Austria, 2009; pp. 51–61.
23. Cornelis, N.; Leibe, B.; Cornelis, K.; van Gool, L. 3D urban scene modeling integrating recognition and reconstruction. *Int. J. Comput. Vis.* **2008**, *78*, 121–141.
24. González-Jorge, H.; Riveiro, B.; Armesto, J.; Arias, P. Standard artifact for the geometric verification of terrestrial laser scanning systems. *Opt. Laser Technol.* **2011**, *43*, 1249–1256.
25. Vaaja, M.; Hyyppä, J.; Kukko, A.; Kaartinen, H.; Hyyppä, H.; Alho, P. Mapping topography changes and elevation accuracies using a mobile laser scanner. *Remote Sens.* **2011**, *3*, 587–600.
26. Arayici, Y. An approach for real world data modelling with the 3D terrestrial laser. *Autom. Constr.* **2007**, *16*, 816–829.
27. Buckley, S.J.; Howell, J.A.; Enge, H.D.; Kurz, T. Terrestrial laser scanning in geology: Data acquisition, processing and accuracy considerations. *J. Geol. Soc.* **2008**, *165*, 625–638.
28. Pu, S. Automatic Building Modelling from Terrestrial Laser Scanning. In *Advances in 3D Geoinformation Systems*; Springer: Berlin/Heidelberg, Germany, 2008; pp. 147–160.
29. Pu, S.; Vosselman, G. Knowledge based reconstruction of building models from terrestrial laser scanning data. *ISPRS J. Photogramm. Remote Sens.* **2009**, *64*, 575–584.
30. Hyyppa, J.; Jaakkola, A.; Hyyppa, H.; Kaartinen, H.; Kukko, A.; Holopainen, M.; Zhu, L.; Vastaranta, M.; Kaasalainen, S.; Krooks, A.; *et al.* Map Updating and Change Detection Using Vehicle-Based Laser Scanning. In Proceedings of the Urban Remote Sensing Event, 2009 Joint, Shanghai, China, 20–22 May 2009.
31. Barber, D.; Mills, J.; Smith-Voysey, S. Geometric validation of a ground-based mobile laser scanning system. *ISPRS J. Photogramm. Remote Sens.* **2008**, *63*, 128–141.
32. Puente, I.; Gonzales-Jorge, H.; Riveiro, B.; Arias, P. Accuracy verification of the Lynx Mobile Mapper system. *Opt. Laser Technol.* **2013**, *45*, 578–586.
33. Beraldin, J.-A.; Picard, M.; El-Hakim, S.F.; Godin, G.; Valzano, V.; Bandiera, A.; Latouche, C. Virtualizing a Byzantine Crypt by Combining High-Resolution Textures with Laser Scanner 3D Data. In Proceedings of the VSMM 2002, Gyeongju, Korea, 25–27 September 2002.
34. Voigt, A.; Martens, B. Development of 3D Tactile Models for the Partially Sighted to Facilitate Spatial Orientation. In Proceedings of the 24th eCAADe Conference, Volos, Greece, 6–9 September 2006.
35. Balzani, M.; Santopuoli, N.; Grieco, A.; Zaltron, N. Laser Scanner 3D Survey in Archaeological Field: The Forum of Pompeii. In Proceedings of International Conference on Remote Sensing Archaeology, Beijing, China, 18–21 October 2004.
36. Reznicek, J.; Pavelka, K. Culture Heritage Preservation with Optical Correlation Scanner. In Proceedings of the 22nd CIPA Symposium, Kyoto, Japan, 11–15 October 2009.
37. Sansoni, G.; Trebeschi, M.; Docchio, F. State-of-the-art and applications of 3D imaging sensors in industry, cultural heritage, medicine, and criminal investigation. *Sensors* **2009**, *9*, 568–601.
38. Schwarzbach, F.; Sarjakoski, T.; Oksanen, J.; Sarjakoski, L.T.; Weckman, S. Physical 3D Models from LIDAR Data as Tactile Maps for Visually Impaired Persons. In *True-3D in Cartography*; Springer: Berlin/Heidelberg, Germany, 2012; pp. 169–183.

39. Rase, W.-D. Visualization of Cartographic Surfaces Using 3D Printing and Subsurface Engraving. Available online: http://www.bbsr.bund.de/cln_016/nn_340582/BBSR/DE/Raumbeobachtung/DE/Raumbeobachtug/Werkzeuge/Visualisierung/Veroeffentlichungen__Artikel/Veroeffentlichungen__Downloads. html (accessed on 12 December 2013).
40. Valentan, B.; Brajlih, T.; Drstvensek, I.; Balic, J. Basic solutions on shape complexity evaluation of STL data. *J. Achiev. Mater. Manuf. Eng.* **2008**, *26*, 73–80.
41. ZPrinter® 450. Available online: http://www.zcorp.com/en/Products/3D-Printers/ZPrinter-450/spage.aspx (accessed on 3 December 2013).
42. Kukko, A.; Kaartinen, H.; Hyyppä, J.; Chen, Y. Multiplatform mobile laser scanning: Usability and performance. *Sensors* **2012**, 12, 11712–11733.